SHELL MODEL OF TURBULENT VISCOSITY FOR THE BOUNDARY LAYER

D.G. Selukov[1] and R.A. Stepanov[1,2]

[1]*Institute of Continuous Media Mechanics UB RAS, Perm, Russian Federation*
[2]*Perm National Research Polytechnic University, Perm, Russian Federation*

The problem of numerical simulation of developed turbulent flows is usually reduced to the choice of one or another closure of the mean field equations. It is difficult to find a universal solution to this issue; nevertheless, the development of an approach based on general principles remains an active research topic. This paper proposes a model of turbulent viscosity described in terms of the characteristics of velocity field fluctuations calculated on the basis of shell models. These models correctly reproduce the distribution of the turbulent energy across scales and spectral energy fluxes for hydrodynamic flows of various physical natures. Shell models are constructed using symmetry properties and conservation laws of the complete system of equations, as well as an assumption of homogeneity and isotropy of turbulence. Phenomenological relations implying specific spectral laws are not involved. In the developed approach, we attempted to determine the turbulent viscosity while maintaining the universality and flexibility of shell models. The resulting mathematical formulation is a set of models for large (mean field equation) and small (cascade model) scales, as well as closing relations. The model implements energy conjugation of variables of different scales, which provides a nonlinear relation of fields at different levels. Considering the influence of the mean field on the energy distribution of turbulent fluctuations is a distinctive feature of the proposed approach. Numerical solutions are obtained for flow in a plane infinite channel at various Reynolds numbers. The obtained results are consistent with modern concepts of the logarithmic profile of the velocity field in the boundary layer. The physical meaning of the model parameters is substantiated. Asymptotic solutions that qualitatively correspond to the Prandtl model are found.

Key words: numerical simulation of turbulence, shell models, boundary layer

1. Introduction

The modeling of turbulent gas and hydrodynamic flows is in demand in various fields of science and engineering. Direct numerical simulation of the equations of motion of gas or fluid at large Reynolds numbers is limited by computational resources and, in fact, is redundant when only calculating the mean field is of interest. The theory of turbulence combines a wide range of approaches and methods for describing turbulence [1]. Many of them have been infused from the related fields of nonlinear physics and computational mathematics. The facilities of modern numerical computations and experimental measurements make it possible to perfect theoretical models and numerical algorithms. The effective combination of these methods for simulating a turbulent boundary layer shows that the mean velocity, Reynolds stresses, and qualitative and quantitative characteristics of coherent structures can be effectively reproduced at reasonable computational costs [2]. Experimental observations are usually used for calibrating constitutive equations and improving the accuracy of computations. The application of machine learning strategies based on numerical simulation data and laboratory measurements offers new prospects for the classical issue of mathematical description of turbulence [3].

With all the diversity of approaches available for modeling turbulent flows, fields are commonly split into mean and fluctuating parts, and the derivation of equations for determining their joint evolution. The Reynolds stress tensor $\boldsymbol{\tau} = \langle \mathbf{v'v'} \rangle$ inevitably appears in the equation of the mean velocity field $\mathbf{V}$ as the average influence of turbulent fluctuations $\mathbf{v'}$. The search for the term $\boldsymbol{\tau}$ dependent on the mean field is reduced to the well-known closure problem, which has not yet had a universal solution. The introduction of turbulence into the mathematical statement is based on one or another expression of the Reynolds stress tensor through model representations of the turbulent field. In the simplest case of an incompressible fluid, the deviatoric part of the Reynolds stress tensor depends on the strain tensor of the mean velocity field (that is, the Boussinesq hypothesis is accepted).

In this case, the influence of turbulent fluctuations on the mean field is exerted through turbulent viscosity ν_t, which is not related to the fluid properties:

$$\boldsymbol{\tau} = \langle \mathbf{v}' \cdot \mathbf{v}' \rangle \mathbf{I}/3 - \nu_t \left(\nabla \mathbf{V} + \nabla \mathbf{V}^{\mathrm{T}} \right), \tag{1}$$

where $\mathbf{I}$ is the identity tensor. To calculate the value of ν_t, it is necessary to know the statistical properties of $\mathbf{v}'$. Starting from some scale, the energy spectrum of the fluctuations can be represented by Kolmogorov's "–5/3" spectrum law

$$\mathcal{E}(k) = C_K D^{2/3} k^{-5/3}, \tag{2}$$

which works well under conditions of homogeneity and isotropy (here, $\mathcal{E}(k)$ is the spectral density of the turbulent fluctuation energy with wavenumber k, C_K is the Kolmogorov constant, and D is the energy dissipation rate that is considered independent of the wavenumber in an inertial interval). However, the ratio of the dissipation rate to the turbulent scale energy can essentially change under the influence of additional factors, such as the magnetic field, global rotation or buoyancy force. The control parameters responsible for these factors can also vary by many orders of magnitude. Therefore, in the general case, it is necessary to solve the problem of finding $\mathcal{E}(k)$ and resort to the expression for turbulent viscosity [4]:

$$\nu_t \sim c_t \int_{k_0}^{\infty} k^{-3/2} \mathcal{E}(k)^{1/2} \, dk \, . \tag{3}$$

The application of shell models of turbulence seems to be a universal and relatively simple approach for obtaining spectrum distributions of energy in the inertial interval and dissipative scale range for various turbulent systems. The main idea of shell models of turbulence is to construct chains of ordinary differential equations with respect to certain collective variables that describe the dynamics of Fourier modes in a certain range of wavenumbers. The most attractive feature of using models of this type is that, with a small number of unknowns, it is possible to introduce nonlinear interactions of many-scale turbulent structures. This is achieved due to only basic properties of the original hydrodynamics equations, namely, the kind of nonlinearity and conservation laws. As a result, it becomes possible to simulate the cascade process of spectrum energy transfer in all possible physical configurations without introducing any phenomenological equation of type (2).

The first versions of shell models of hydrodynamics were proposed as early as the 1970s (see [5–9]) and included low-dimensional systems that reproduced the major features of turbulence. The three most famous shell models, described by the GOY [7, 10] or the Sabra models [11–13], describe local interactions between two neighboring shells [8] or three nearest shells. An even more complicated model was constructed in [14] using the wavelet transform. The development of shell model concepts took place in parallel with the discovery of various fine properties of turbulence, for example, anomalous scaling of structural functions. The scaling characterizes the intermittent dynamics of cascade processes [15–18]. Later, special attention was given to shell models of magnetohydrodynamic turbulence [19], which stand out for the variety of possible solutions and their applications to problems of geo- and astrophysics.

The idea of using shell models to estimate turbulent viscosity was previously proposed in a number of papers [20–23]. One of those works [24] included a method for constructing a two-scale model for the turbulent transport of a magnetic field in a rotating disk. The model includes an equation for the mean magnetic field and a shell model of MHD-turbulence, which makes it possible to calculate turbulent transport coefficients in the mean field equation. In [25], a model of near-wall turbulent

flows was proposed. The area near the wall is divided into zones; the further from the wall, the larger the zone size. In fact, the decomposition of the velocity field in terms of a hierarchical wavelet basis has been introduced. The role of shell models in the abovementioned publications was to consider the interactions of flow velocity fluctuations in different size zones with different turbulence scales and to calculate the turbulent energy density. This approach is called "the multizone shell model".

The purpose of this work is to construct a two-level model of the near-wall boundary layer that directly links finite difference equations of the mean field and the equations of shell models formulated for each node. Moreover, it is desirable to maintain the simplicity of construction, bearing in mind the further prospect of generalizing the model to the case of spiral turbulence. The properties of spiral turbulence and related hydrodynamics effects, primarily the reverse cascade, have attracted attention in topical studies [26-29].

2. Two-level model of the near-wall boundary layer

In the two-level model, the large-scale level describes the evolution of the mean fields. Let us consider a flow in a flat infinite channel of thickness $2h$ with boundaries perpendicular to the axis z. The flow is under a homogeneous pressure gradient acting along the channel x-axis. The Navier–Stokes equation for the mean value x-component velocity field $V(t,z)$ can be transformed to a dimensionless form:

$$\partial_t V(t,z) = -p + \partial_z \left(\left(\mathrm{Re}^{-1} + v_t(t,z) \right) \partial_z V(t,z) \right), \tag{4}$$

where $\mathrm{Re} = hV_c/v$ is the Reynolds number, p is the pressure gradient, and $v_t(t,z)$ is the turbulence viscosity setting in hV_c the characteristic unit (V_c is the characteristic velocity in the middle of the flow).

The small-scale level of the model is responsible for describing small-scale structures of the flow. The energy of the fluctuations in the mean velocity field occurs in both physical and spectral spaces in turbulent flow. Consequently, the spectral density of the velocity fluctuations is set as a function of z, which must satisfy the balance equation:

$$\partial_t \mathcal{E}(t,z,k) = T(t,z,k) - D(t,z,k) + I(t,z,k), \tag{5}$$

where T is the term responsible for the nonlinear interaction of energy exchange between the scale corresponding to k and other scales, D is the spectral density of the energy dissipation rate, and I is the spectral density of the energy inflow "lost" from the mean field.

The equations of two levels (4) and (5) of the model are not completely separated. The small-scale variables are entered (4) through $v_t(t,z)$, and the large-scale variables are entered (5) through $I(t,z,k)$. It is possible to relate the models in terms of physical considerations. For the large-scale range L, the law of energy conservation means that:

$$\int_{k \subset L} I(t,z,k') dk' = v_t(t,z) \left(\partial_z V(t,z) \right)^2 . \tag{6}$$

Eq. (6) and Eq. (3) are the constitutive relations relating to the two levels of the model. Since all the field variables below are time dependent, the corresponding argument is omitted.

3. Numerical model

In this section, a discrete analog of the model equations is introduced, and a computational scheme for numerical simulation is considered.

3.1. Discretization of the mean field equation

Due to the symmetry of the problem with respect to the channel center, equation (4) is solved for one half. Let us split the change range of spatial variable $z \in [0;1]$ (the boundary $z = 0$ is a wall, and the boundary $z = 1$ is the middle of the channel) into M intervals. In the near-wall zone, we condense the grid so that the coordinates of its nodes change according to the power law:

$$z_m = \Delta z_{\min} 2^{m-1}, \qquad 1 \le m \le M_c, \tag{7}$$

where $\Delta z_{\min}$ — the minimum step size near a wall; M_c — the number of intervals until the maximum step is reached $\Delta z_{\max}$, which is defined as

$$M_c = \lceil \log_2 \frac{\Delta z_{\max}}{\Delta z_{\min}} \rceil + 1. \tag{8}$$

For nodes z_m with $m > M_c$, we use a constant step size $\Delta z_{\max}$ until $z = 1$. Thus, the full number of intervals equals

$$M = M_c + \lfloor \frac{1 - z_{M_c}}{\Delta z_{\max}} \rfloor. \tag{9}$$

Then, the length of the arbitrary interval is set by the following formula:

$$\Delta z_m = z_m - z_{m-1}, \qquad 1 \le m \le M, \tag{10}$$

given that $z_0 = 0$.

Let us introduce the mean field value V_m in the interval m:

$$V_m \equiv \Delta z_m^{-1} \int_{z_{m-1}}^{z_m} V(z) \, dz, \tag{11}$$

and write a finite-difference analog of equation (4) in the form:

$$\partial_t V_m = -p + \Delta z_m^{-1} \left(F_m - F_{m-1} \right). \tag{12}$$

Here, the momentum flux at the boundary of the interval m is defined as

$$F_m \equiv \left(\mathrm{Re}^{-1} + v_{tm} \right) \partial_z V_m. \tag{13}$$

The proposed scheme is conservative since the integral change of the momentum depends on the fluxes at the boundary. The finite-difference approximation of the first-order spatial derivative of the velocity at the boundary between the m and $m+1$ intervals has the form:

$$\partial_z V_m = \frac{2(V_{m+1} - V_m)}{\Delta z_{m+1} + \Delta z_m} + O\left(\max\left(\Delta z_m, \Delta z_{m+1}\right)\right). \qquad (14)$$

3.2. Discretization of the spectral transport equations

The mathematical apparatus of shell models seems to be an appropriate basis for describing the evolution of the spectral density of fluctuation energy. Within the framework of this approach, we split the three-dimensional space of wave vectors into spherical shells and apply the hypothesis of homogeneous and isotropic turbulence. Let us introduce one collective variable responsible for the full energy of all fluctuations from the wavenumber range of the shell. We also accept the hypothesis of isotropy, but at the same time, we consider the case of local homogeneity; that is, we describe turbulence by an independent shell model in the vicinity of each node z_m.

We assume that the n-th shell of the shell model at point z_m contains all fluctuations in the range of wavenumbers $\left[k_{m,n-1/2}; k_{m,n+1/2}\right]$, whose energy is

$$E_{m,n} = \Delta z_m \int_{k_{m,n-1/2}}^{k_{m,n+1/2}} \mathcal{E}(z_m, k)\, dk, \qquad 1 \le n \le N. \qquad (15)$$

Here, $\mathcal{E}(z_m, k)$ is the spectral density of energy at wavenumber k and at distance z_m from the wall in the physical space; N is the number of shells. The splitting of wavenumbers $k_{m,n} = \kappa z_m^{-1} \lambda^n$ is carried out considering that as we approach the wall, the maximum possible scale of fluctuation is limited by the distance to the wall. The model parameter κ should obey the consideration of conjugation with the spatial grid, where λ is the split parameter. The number of shells N is taken as it is so that the scale corresponding to the wavenumber $k_{m,N}$ scale is obviously less than the dissipative scale $\propto \mathrm{Re}^{-3/4}$.

The shell variables $U_{m,n}$ take on complex values that are related to energy as

$$E_{m,n} = \Delta z_m \left|U_{m,n}\right|^2 \big/ 2. \qquad (16)$$

The evolution equations of the shell variables can be represented in the general form:

$$\partial_t U_{m,n} = W_{m,n}(U) - \mathrm{Re}^{-1} k_{m,n}^2 U_{m,n} + f_{m,n}, \qquad (17)$$

where $W_{m,n}$ is the bilinear form responsible for describing nonlinear interactions of different scales of the flow, which lead to cascade processes (it is the bilinear form that distinguishes one shell model from another; the specific choice of the form will be shown in the computation section), and $f_{m,n}$ is the spectral force providing the energy inflow into the shell model (hereinafter, it will be called the turbulent force).

3.3. Discretization of connection relations

The turbulent viscosity (3) can be expressed in shell variables $U_{m,n}$:

$$\nu_{tm} = c_t \sqrt{\ln \lambda} \sum_{n=1}^{N_t} k_{m,n}^{-1} \left| U_{m,n} \right|, \tag{18}$$

where c_t is the model parameter and N_t is the number of "viscous" shells that specifies the degree of overlap between the scales of the large-level grid and the shell model.

Let us set the inverse influence of the mean field on the evolution of the turbulent part of the field as the energy balance (6). The rate of energy inflow into the shell model from a large scale in the vicinity of z_m, which belongs to the n-th shell, must be equal to the rate of dissipation of the mean field energy due to turbulence:

$$\left(f_{m,n} U_{m,n}^* + f_{m,n}^* U_{m,n} \right) \big/ 2 = c_t \sqrt{\ln \lambda}\, k_{m,n}^{-1} \left| U_{m,n} \right| \left(\partial_z V_m \right)^2. \tag{19}$$

Then, the expression for the turbulent force providing the equality takes the form:

$$f_{m,n} = \begin{cases} c_t \sqrt{\ln \lambda}\, k_{m,n}^{-1} \dfrac{U_{m,n}}{\left| U_{m,n} \right|} \left(\partial_z V_m \right)^2, & n \le N_t, \\[2ex] 0, & n > N_t. \end{cases} \tag{20}$$

Note that the mean field is specified at the centers of the cells of the spatial grid, and the fluctuation amplitude is specified at the boundaries of the cells.

4. Computational results

In this section, the computational results of applying the proposed turbulent viscosity shell model are shown. The emphasis is placed on scaling the mean velocity profile and turbulent energy at various Reynolds numbers. Let us also analyze the nature of changes in the spectral properties of turbulence with distance from the wall.

For numerical implementation, we use the shell model, which has recently been widely used in research. Its distinguishing feature is that the model makes it possible to correctly describe both the energy and the helicity cascades simultaneously [29]. Its bilinear form is:

$$\begin{aligned} W_n(U) &= ik_n \left(U_{n-1}^2 - U_{n-1}^{*2} + \lambda U_n^* \left(U_{n+1} - U_{n+1}^* \right) - \lambda^2 U_n \left(U_{n+1} + U_{n+1}^* \right) \right) \big/ 2 + \\ &+ ik_n \gamma \left(U_n \left(U_{n-1} + U_{n-1}^* \right) + \lambda U_n^* \left(U_{n-1}^* - U_{n-1} \right) - \lambda^2 \left(U_{n+1}^2 + U_{n+1}^{*2} \right) \right) \big/ 2, \end{aligned} \tag{21}$$

where the model parameter equals $\gamma = \lambda^{-5/2}$ and the variables outside the computational range are fixed: $U_{0,m} = 0$ and $U_{N+1,m} = 0$.

To fulfill the boundary conditions for the symmetry of the velocity field and for no-slip on the wall, the values of the mean field at the corresponding nodes should be as follows:

$$V_0 = 0, \quad V_M = V_{M-1}. \tag{22}$$

In this case, it is necessary to formally assume that $\Delta z_0 = 0$ and $\Delta z_{M+1} = \Delta z_M$. Then, for the turbulent viscosity at the boundaries of the observation area, the following equation is used: $\nu_{t0} = 0$ and $\nu_{tM} = 0$.

All the numerical calculations for the obtained discrete Poiseuille flow model were carried out with the following initial data: $p = -1$, the grid parameters depend on the Reynolds number $\delta'_{\min} = 10^{-1}\text{Re}^{-1}$, $\delta'_{\max} = 0.1$, the shell splitting parameter $\lambda = 1.7555$, the number of shells in each shell model providing a cover of dissipation scale for all the ranges of the considered Reynolds numbers $N = 17$, and the number of cells under turbulent force inflow $N_t = 2$. The evolutionary equations were integrated by the 9th-order implicit Runge–Kutta method in the Wolfram Mathematica 12 package. The computations were carried out until a quasistationary state was established in the turbulent flow.

The first thing that is of interest in the nature of the obtained solutions is the mean field profiles. It is known [30] that for turbulent flows in the area of maximum shear, the velocity field logarithmically depends on the distance to the wall:

$$V\left(z^+\right) = q\log\left(z^+\right) + \tilde{V}, \tag{23}$$

where $z^+ = z\text{Re}$ is the auxiliary variable and q and $\tilde{V}$ are the velocity profile parameters in logarithmic coordinates.

Figure 1 shows the distribution of the mean velocity field for various Reynolds numbers in the range $\text{Re} \in [10, 10^5]$ with model parameters $c_t = 1$ and $\kappa = 1$. A pronounced logarithmic profile is clearly formed at $\text{Re} = 10^5$. In the area $1 \le z^+ \le 10$, there is a transition to a viscous layer. At larger values, the velocity profile deviates from the logarithmic form due to the chosen boundary condition (22).

The developed shell model of turbulent viscosity makes it possible to study the structure of the turbulent field at different levels. Thus, at the small-scale level of the model, we observe a change in the nature of cascade processes as one approaches the wall. Figure 2 shows the temporal evolution of the turbulent energy. Statistically stationary quasiperiodic fluctuations are clearly expressed in the region of the turbulent layer.

By fixing the value z and averaging over time, one can obtain spectral distributions of energy (Figure 3). The formation of a cascade energy transfer is manifested in the presence of the inertial interval of the spectrum section with the $k^{-2/3}$ law, which corresponds to the "$-5/3$" law for the spectral density of the energy.
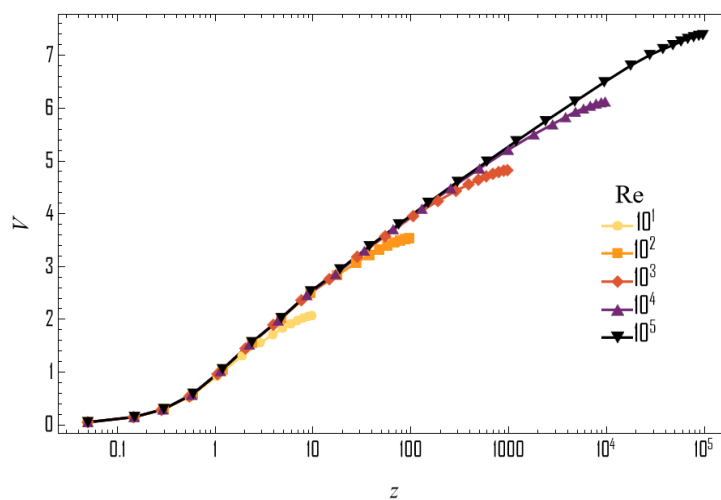
Fig. 1. Mean velocity field profile at the various Reynolds numbers and fixed model parameters $c_t = 1$ and $\kappa = 1$
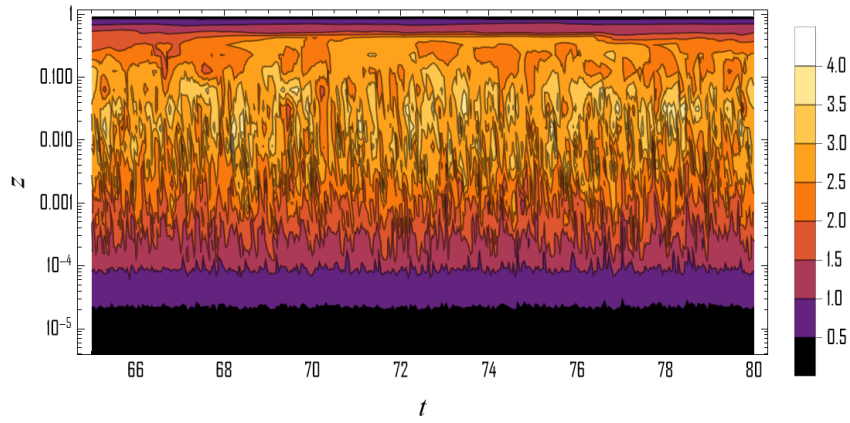
Fig. 2. The dependence of the fluctuation energy on the time and distance to the wall at fixed $\mathrm{Re} = 10^5$
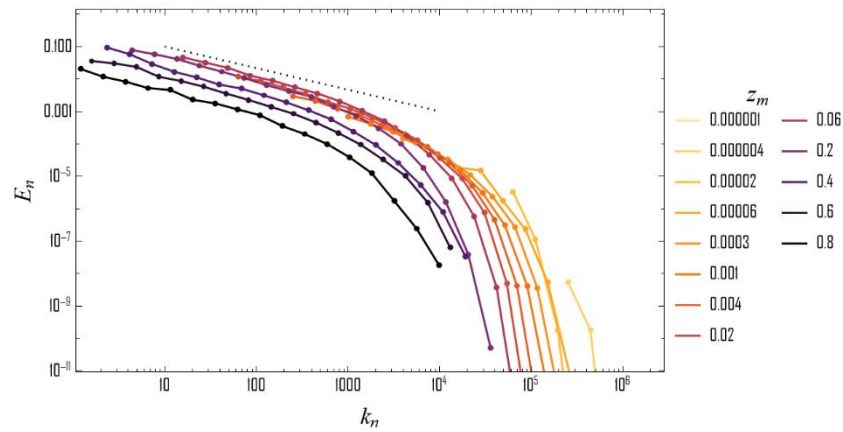
Fig. 3. Fluctuation spectra at $\mathrm{Re} = 10^5$ at various distances to the wall z_m; the dotted line corresponds to the law $E_n \sim k_n^{-2/3}$ Спектры пульсаций при $\mathrm{Re} = 10^5$ на разных расстояниях до стенки z_m; пунктирная линия соответствует закону $E_n \sim k_n^{-2/3}$

Of special interest is the distribution of the turbulent viscosity and the mean field dissipation rate since they play a key role in matching the levels of the model. The turbulent viscosity profiles are shown in Figure 4a. There is a laminar layer with negligible turbulence viscosity, which increases with increasing distance to the wall. This behavior is pronounced at high Reynolds numbers. For low flows, the turbulent viscosity does not significantly exceed the kinematic viscosity. Figure 4b shows the mean field energy dissipation rate, which reaches a maximum at $z^+ \approx 1$ and is strictly normalized by the Reynolds number.
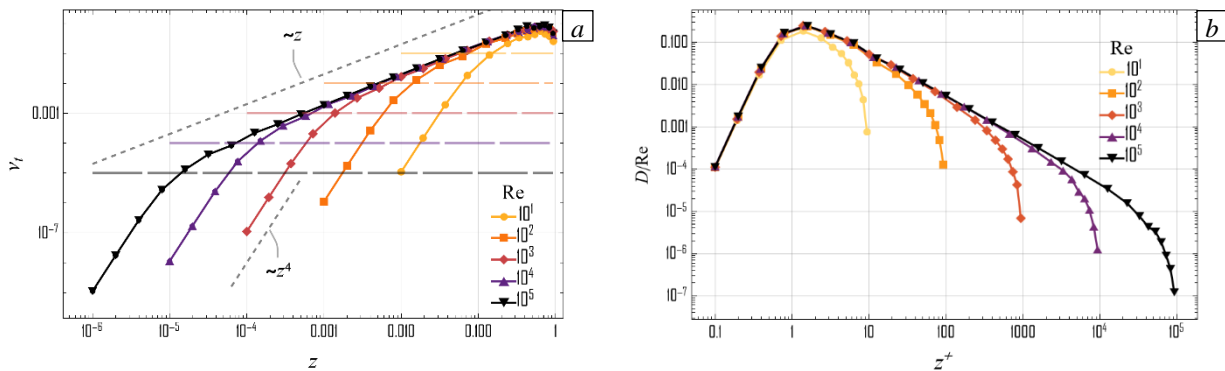
Fig. 4. Spatial distributions of the turbulent viscosity (a) and turbulent energy dissipation rate (b) at various Reynolds numbers; dotted lines sign corresponded levels of viscosity ν

5. Constants and parameters relations between the shell model of turbulent viscosity and the Prandtl model

In this section, a comparison is made between the developed shell model and the well-known Prandtl model of turbulent viscosity based on the idea of the mixing length [1]:

$$\nu_t^p(z) = c_p z^2 \left| \partial_z V \right|, \tag{24}$$

c_p — Prandtl constant.

For the turbulent viscosity related to a certain shell, in the vicinity of point z_m (the index m is omitted for brevity), from (3), and after substituting the appropriate limits of the wavenumber boundaries, we obtain the expression:

$$\nu_{tn} \sim c_t \int_{k_{n-1/2}}^{k_{n+1/2}} k^{-3/2} \mathcal{E}^{1/2} dk \sim c_t \ln \lambda k_n^{-1/2} \mathcal{E}^{1/2}. \tag{25}$$

Using the Kolmogorov law (2) for expression (25), summing the contributions to the turbulent viscosity of each shell (we assume $\nu_t = \sum_n \nu_{tn}$) and considering the dissipation term from the right part of equation (6), we can obtain a mathematical formulation of the theoretical prediction of the turbulent viscosity expression for the present model:

$$\nu_t(z) = \left(c_t \alpha_\lambda \sqrt{C_K} \right)^{3/2} \kappa^{-2} z^2 \left| \partial_z V \right|, \tag{26}$$

where $\alpha_\lambda = \ln \lambda \sum_{n=1}^{N_t} \lambda^{-4(n-1)/3}$.

Expression (26) is equivalent to the Prandtl model (24) with the constant

$$c_p = \left(c_t \alpha_\lambda \sqrt{C_K} \right)^{3/2} \kappa^{-2}. \tag{27}$$

Let us find the relation between c_p and parameter q of the logarithmic profile (23). Considering the mean velocity field equation without kinematic viscosity (ν is neglected):

$$\partial_t V(z) = -p + \partial_z \left(\nu_t^p(z) \partial_z V(z) \right). \tag{28}$$

The analytical solution for the velocity field with the condition $\partial_t V(z=1)$ can be obtained from equations (24) and (28) and has the form:

$$V(z) = 2\sqrt{-p/c_p} \left(\sqrt{1-z} - \mathrm{arth}\left(\sqrt{1-z} \right) + C \right). \tag{29}$$

The Taylor series expansion of this solution near zero gives the expression:

$$V(z) = \sqrt{-p/c_p} \left(\log z + (2 - 2\log 2 + C) - \frac{z}{2} - \frac{z^2}{16} - \frac{z^3}{48} - \frac{5z^4}{512} + o(z^5) \right), \tag{30}$$

which has a logarithmic part. Near the wall, we have $q \sim c_p^{-1/2}$, and using relation (27) for the shell models, the formula takes the form:

$$q \sim \left(c_t \sqrt{C_K} \right)^{-3/4} \kappa. \tag{31}$$

There is a layer near the wall where the turbulent viscosity is negligible compared to the kinematic viscosity since turbulent eddies are limited in scale by the distance to the wall. Let us determine the thickness of the viscous layer through the distance Δz_v, at which the turbulent viscosity is equal to the kinematic viscosity:

$$v_t \left(\Delta z_v \right) = \mathrm{Re}^{-1}. \tag{32}$$

Within the viscous layer, due to the low turbulent viscosity, the turbulent flux is also small. This is confirmed by the computational results (see Figure 3). We assume that most of the energy inflowing into the shell models immediately dissipates; then,

$$v_{tm} \left| \partial V_m \right|^2 = \mathrm{Re}^{-1} k_{m,1}^2 \left| U_{m,1} \right|^2. \tag{33}$$

By substituting expression (33) into (18), we obtain an estimate of the turbulent viscosity in the near-wall area:

$$v_t = c_t^2 \kappa^{-4} \mathrm{Re} \left(\partial_z V \right)^2. \tag{34}$$

The turbulent viscosity scaling is represented in the shell model near the wall as $v_t(z) \sim z^4$, and in the Prandtl model, in accordance with (24), the scaling is $v_t^p(z) \sim z^2$. For a layer with a logarithmic velocity profile, the invariant scaling for both models is dependent on $v_t(z) \sim z$. Finally, for the thickness of the viscous boundary layer near the wall, we have the following dependence:

$$\Delta z_v \sim \kappa \left(c_t \mathrm{Re} \left| \partial_z V \right| \right)^{-1/2}. \tag{35}$$
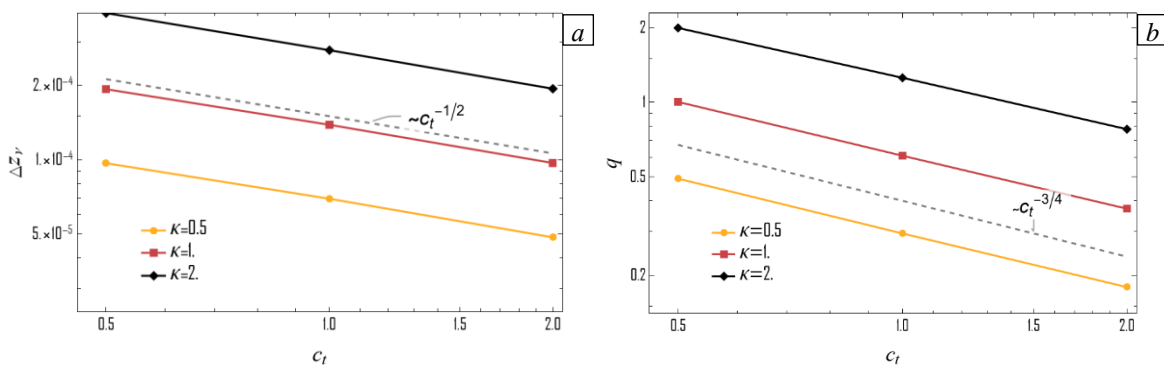
Fig 5. Viscous layer width (*a*) and the slope of logarithmic profile (*b*) dependences from c_t at $\mathrm{Re} = 10^4$ with various values of shell model parameter κ

A number of numerical computations were carried out at $\mathrm{Re} = 10^5$ and for all possible pairs of model parameters from the lists $\kappa \in \{0.5, 1, 2\}$ and $c_t \in \{0.5, 1, 2\}$. For each computation, the coefficient q is calculated in accordance with formula (23), and the thickness of the viscous layer is

calculated by formula (32). Figure 5 shows the calculated dependences of the thickness of the viscous layer and the slopes of the logarithmic velocity profile on the model parameter c_t at various fixed values of κ. The numerically revealed power laws are in agreement with the theoretical estimates (31) and (35).

6. Discussion of the results and conclusions

The problem of a flow with the formation of a turbulent boundary layer, when solved in its entirety, includes taking into account the anisotropy and inhomogeneity of the properties of the velocity field fluctuations. Anisotropy arises due to the predominant motion of the fluid along the channel, while inhomogeneity occurs due to the presence of a solid wall with the no-slip boundary condition. The model is constructed using the grid-shell approach. The model describes inhomogeneity by introducing the spatial dependence of the shell variables so that the turbulence still remains locally homogeneous for each shell model. This is achieved by increasing the number of shells N to such an extent that the scale of the mean field inhomogeneity becomes much larger than the scales represented by the shell variables. Strict consideration of anisotropy requires the development of new anisotropic shell models. Successful attempts at anisotropic turbulence simulation have already taken place; namely, the influence of the Coriolis force [31, 32], buoyancy [33], and external magnetic field [34] on the turbulent flow of electrically conducting fluids has been considered.

The results obtained show that the existing shell models can be applied both for studying the developed turbulence regime and for the transition of the flow to conditions when dissipation prevails over nonlinearity. In the absence or at a low level of energy inflow, the shell model degenerates, and a cascade does not arise. In addition, the performance of the shell model can deteriorate in the presence of an energy inflow but also due to the smallness of the scale under inflow. For the current problem of analyzing turbulent viscosity, the inflow in shell models is determined by the mean field gradient. Figure 4 shows low-energy shell models near the wall, despite the high gradient of the mean velocity in the near-wall flow region. This is due to the limitation of the scales of fluctuations by the distance to the wall. It is clear that these two factors can be included in the local Reynolds number depending on z. The critical value of this number determines the presence or absence of a cascade process.

The shell model, located in the very center of the flow, degenerates due to the zero mean velocity gradient. In real flows, there is a mechanism for the transfer of turbulent energy across space, so fluctuations are also present at a locally zero gradient of the mean field. Nevertheless, qualitatively consistent results were obtained for the experimental plots for the mean velocity field. In this paper, it is important to describe the boundary and the logarithmic velocity field. The question of the applicability of shell models, considering all the factors, requires further research.

The theoretical profile of the turbulent viscosity (26) was determined, and the computational results of the profile correspond to the results of the Prandtl model. The proposed model is essentially two-parametric and allows independent control of the slope of the logarithmic profile of the mean velocity field and the thickness of the viscous layer. The Prandtl model contains only one parameter; thus, the abovementioned characteristics of this model are related.

Another advantage of the proposed model is the physicality of the connection between the large-scale and small-scale levels of the model. All the phenomenology of shell models is directed toward an adequate reproduction of the statistical properties of turbulence. Given the flexibility and wide applicability of shell models, one can hope for a fairly efficient transition to shell models that will be able to describe the turbulence of hydrodynamic flows in the presence of additional physical fields.

From a computational point of view, carrying out calculations based on the proposed model requires significant computing resources. This is due to two circumstances. First, dozens of additional (cascade) variables must be introduced for each spatial node. Second, the step of integrating the entire system of equations is limited by the minimum characteristic time of the turbulent spectrum evolution. This is a significant disadvantage of the proposed approach, and in practical terms, it will concede the positions to widely used approaches that have already become traditional in turbulence simulation,

such as RANS и LES. However, when calculating a turbulent boundary layer, these approaches can yield significant systematic mismatches, for example, due to the effect of the log-layer mismatch (LLM) [35]. The LLM is related to the fact that it is not possible to realize a smooth transition from the area with resolved and unresolved scales of turbulence. By careful comparison of LES results with experimental measurements and direct numerical simulation, patches can be added at the expense of the latter, reducing the influence of LLM [36]. When solving problems in which the spectral properties of turbulence are not known a priori, the semiempirical model proposed in this paper, which resolves an arbitrary nonstationary turbulent spectrum, will provide a more accurate result.

References

1. Frik P.G. *Turbulentnost': podkhody i modeli*. M.-Izhevsk: Regulyarnaya i khaoticheskaya dinamika, 2010. 332 p.
2. Tazraei P., Girimaji S.S. Scale-resolving simulations of turbulence: Equilibrium boundary layer analysis leading to near-wall closure modeling. *Phys. Rev. Fluids*, 2019, vol. 4, 104607. http://doi.org/10.1103/PhysRevFluids.4.104607
3. Duraisamy K., Iaccarino G., Xiao H. Turbulence modeling in the age of data. *Annu. Rev. Fluid Mech.*, 2019, vol. 51, pp. 357-377. http://doi.org/10.1146/annurev-fluid-010518-040547
4. Yokoi N. Turbulence, transport and reconnection. *Topics in magnetohydrodynamic topology, reconnection and stability theory*, ed. D. MacTaggart, A. Hillier. Springer, 2020. P. 177-265. http://doi.org/10.1007/978-3-030-16343-3_6
5. Obukhov A.M. O nekotorykh obshchikh kharakteristikakh uravneniy dinamiki atmosfery [Some general characteristic equations of the dynamics of the atmosphere]. *Izvestiya of the Academy of Sciences of the USSR. Atmospheric and Oceanic Physics*, 1971, vol. 7, no. 7, pp. 695-704.
6. Lorenz E.N. Low order models representing realizations of turbulence. *J. Fluid Mech.*, 1972, vol. 55, pp. 545-563. http://doi.org/10.1017/S0022112072002009
7. Gledzer E.B. System of hydrodynamic type admitting two quadratic integrals of motion. *Sov. Phys. Dokl.*, 1973, vol. 18, pp. 216-217.
8. Desnyansky V.N., Novikov E.A. The evolution of turbulence spectra to the similarity regime. *Izvestiya of the Academy of Sciences of the USSR. Atmospheric and Oceanic Physics*, 1974, vol. 10, pp. 127-136.
9. Siggia E.D. Origin of intermittency in fully developed turbulence. *Phys. Rev. A*, 1977, vol. 15, pp. 1730-1750. http://doi.org/10.1103/PhysRevA.15.1730
10. Yamada M., Ohkitani K. Lyapunov spectrum of a chaotic model of three-dimensional turbulence. *J. Phys. Soc. Jpn.*, 1987, vol. 56, pp. 4210-4213. http://doi.org/10.1143/JPSJ.56.4210
11. L'vov V.S., Podivilov E., Pomlyalov A., Procaccia I., Vandembroucq D. Improved shell model of turbulence. *Phys. Rev. E*, 1998, vol. 58, pp. 1811-1822. http://doi.org/10.1103/PhysRevE.58.1811
12. L'vov V.S., Podivilov E., Procaccia I. Hamiltonian structure of the Sabra shell model of turbulence: Exact calculation of an anomalous scaling exponent. *EPL*, 1999, vol. 46, pp. 609-612. http://doi.org/10.1209/epl/i1999-00307-8
13. Ditlevsen P.D. Symmetries, invariants, and cascades in a shell model of turbulence. *Phys. Rev. E*, 2000, vol. 62, pp. 484-489. http://doi.org/10.1103/PhysRevE.62.484
14. Benzi R., Biferale L., Tripiccione R., Trovatore E. (1+1)-dimensional turbulence. *Phys. Fluids*, 1997, vol. 9, pp. 2355-2363. http://doi.org/10.1063/1.869356
15. Frisch U. *Turbulence*. Cambridge University Press, 1995. 296 p.
16. Bohr T., Jensen M.H., Vulpiani A., Paladin G. *Dynamical systems approach to turbulence*. Cambridge University Press, 1998. 350 p.
17. Pope S.B. *Turbulent flows*. Cambridge University Press, 2000. 771 p.
18. Biferale L. Shell models of energy cascade in turbulence. *Ann. Rev. Fluid Mech.*, 2003, vol. 35, pp. 441-468. http://doi.org/10.1146/annurev.fluid.35.101101.161122
19. Plunian F., Stepanov R., Frick P. Shell models of magnetohydrodynamic turbulence. *Phys. Rep.*, 2013, vol. 523, pp. 1-60. http://doi.org/10.1016/j.physrep.2012.09.001
20. Frick P., Reshetnyak M., Sokoloff D. Combined grid-shell approach for convection in a rotating spherical layer. *EPL*, 2002, vol. 59, pp. 212-217. http://doi.org/10.1209/epl/i2002-00228-6

21. Frick P., Reshetnyak M., Sokoloff D. Cascade models of turbulence for the Earth's liquid core. *Dokl. Earth Sci.*, 2002, vol. 387, pp. 988-991.

22. Reshetnyak M.Yu., Shteffen B. Kaskadnyye modeli v bystrovrashchayushchikhsya dinamo-sistemakh [Cascade models in rapidly rotating dynamo systems]. *Vych. met. programmirovaniye – Numerical Methods and Programming*, 2006, vol. 7, no. 1, pp. 85-92.

23. Frick P., Stepanov R., Sokoloff D. Large- and small-scale interactions and quenching in an α^2-dynamo. *Phys. Rev. E*, 2006, vol. 74, 066310. http://doi.org/10.1103/PhysRevE.74.066310

24. Stepanov R.A., Frick P.G., Sokoloff D.D. Coupling of mean-field equation and shell model of turbulence in the context of galactic dynamo problem. *Vychisl. mekh. splosh. sred – Computational continuum mechanics*, 2008, vol. 1, no. 4, pp. 97-108. http://doi.org/10.7242/1999-6691/2008.1.4.43

25. L'vov V.S., Pomyalov A., Tiberkevich V. Multizone shell model for turbulent wall bounded flows. *Phys. Rev. E*, 2003, vol. 68, 046308. http://doi.org/10.1103/PhysRevE.68.046308

26. Plunian F., Teimurazov A., Stepanov R., Verma M.K. Inverse cascade of energy in helical turbulence. *J. Fluid Mech.*, 2020, vol. 895, A13. http://doi.org/10.1017/jfm.2020.307

27. Sadhukhan S., Samuel R., Plunian F., Stepanov R., Samtaney R., Verma M.K. Enstrophy transfers in helical turbulence. *Phys. Rev. Fluids*, 2019, vol. 4, 084607. http://doi.org/10.1103/PhysRevFluids.4.084607

28. Stepanov R., Golbraikh E., Frick P., Shestakov A. Helical bottleneck effect in 3D homogeneous isotropic turbulence. *Fluid Dyn. Res.*, 2018, vol. 50, 011412. http://doi.org/10.1088/1873-7005/aa782e

29. Stepanov R., Golbraikh E., Frick P., Shestakov A. Hindered energy cascade in highly helical isotropic turbulence. *Phys. Rev. Lett.*, 2015, vol. 115, 234501. http://doi.org/10.1103/PhysRevLett.115.234501

30. Schlichting H. *Grenzschicht-Theorie* [Boundary Layer Theory]. Verlag G. Braun. Karlsruhe, 1958. 603 p.

31. Shestakov A.V., Stepanov R.A., Frick P.G. Influence of rotation on cascade processes in helical turbulence. *Vychisl. mekh. splosh. sred – Computational continuum mechanics*, 2012, vol. 5, no. 2, pp. 193-198. http://doi.org/10.7242/1999-6691/2012.5.2.23

32. Shestakov A.V., Stepanov R.A., Frick P.G. On cascade energy transfer in convective turbulence. *J. Appl. Mech. Tech. Phys.*, 2017, vol. 58, pp. 1171-1180. https://doi.org/10.1134/S0021894417070094

33. Gledzer E.B. Rotation and helicity effects in cascade models of turbulence. *Dokl. Phys.*, 2008, vol. 53, pp. 216-220. https://doi.org/10.1134/S1028335808040101

34. Plunian F., Stepanov R. Cascades and dissipation ratio in rotating magnetohydrodynamic turbulence at low magnetic Prandtl number. *Phys. Rev. E*, 2010, vol. 82, 046311. http://doi.org/10.1103/PhysRevE.82.046311

35. Nikitin N.V., Nicoud F., Wasistho B., Squires K.D., Spalart P.R. An approach to wall modeling in large-eddy simulations. *Phys. Fluids*, 2000, vol. 12, pp. 1629-1632. http://doi.org/10.1063/1.870414

36. Yang X.I.A., Park G.I., Moin P. Log-layer mismatch and modeling of the fluctuating wall stress in wall-modeled large-eddy simulations. *Phys. Rev. Fluids*, 2017, vol. 2, 104601. http://doi.org/10.1103/PhysRevFluids.2.104601